Nat Chem Biol. Author manuscript; available in PMC 2015 December 30.

Published in final edited form as:
Nat Chem Biol. 2015 May ; 11(5): 347–354. doi:10.1038/nchembio.1790.

siRNA screen identifies QPCT as a druggable target for Huntington's disease

Maria Jimenez-Sanchez[1], **Wun Lam**[1,2], **Michael Hannus**[#3], **Birte Sönnichsen**[#3], **Sara Imarisio**[#1,2], **Angeleen Fleming**[#1,4], **Alessia Tarditi**[6,#], **Fiona Menzies**[1], **Teresa Ed Dami**[1,4,5], **Catherine Xu**[1,4], **Eduardo Gonzalez-Couto**[6,€], **Giulia Lazzeroni**[6], **Freddy Heitz**[6,£], **Daniela Diamanti**[6], **Luisa Massai**[6], **Venkata P. Satagopam**[7,8], **Guido Marconi**[6,$], **Chiara Caramelli**[6,&], **Arianna Nencini**[6], **Matteo Andreini**[6], **Gian Luca Sardone**[6], **Nicola P. Caradonna**[6], **Valentina Porcari**[6], **Carla Scali**[6], **Reinhard Schneider**[7,8], **Giuseppe Pollio**[6], **Cahir J. O'Kane**[2], **Andrea Caricasole**[6,^,*], and **David C. Rubinsztein**[1,*]

[1]Department of Medical Genetics, University of Cambridge, Cambridge Institute for Medical Research, Addenbrooke's Hospital, Hills Road, Cambridge CB2 0XY, UK

[2]Department of Genetics, University of Cambridge, Cambridge CB2 3EH, UK

[3]Cenix BioScience GmbH, Tatzberg 47, 01307 Dresden, Germany

[4]Department of Physiology, Development and Neuroscience, University of Cambridge, Downing Street, Cambridge, UK, CB2 3EG.

[5]Department of Neuroscience, Psychology, Drug Research and Child Health, Division of Pharmacology and Toxicology, University of Florence, Florence, Italy

[6]Siena Biotech. Strada del Petriccio e Belriguardo, 35 53100 Siena, Italy

[7]Structural and Computational Biology, EMBL, Meyerhofstr.1, 69117, Heidelberg, Germany

[8]Luxembourg Centre for Systems Biomedicine (LCSB), University of Luxembourg, Campus Belval, House of Biomedicine, 7 avenue des Hauts-Fourneaux, L-4362 Esch-sur-Alzette, Luxembourg

[#] These authors contributed equally to this work.

Abstract

[*]Address correspondence to: David C. Rubinsztein – Tel: +44 (0)1223 762608, Fax: +44 (0)1223 331206, dcr1000@hermes.cam.ac.uk or to Andrea Caricasole A.Caricasole@irbm.it.
[#]Current address: TPV GmbH, Messerschmittstr. 1+3 , D-80992 München, Germany
[£]Current address: GenKyoTex S.A.,16 Chemin des Aulx, CH-1228,Geneva, Switzerland
[€]Current address: Integromics S.L., Santiago Grisolía, 2 E-28760 Tres Cantos (Madrid)
[$]Current address: Autifony S.r.l., Via Fleming, 437135 Verona (VR), Italy
[&]Current address: Novartis Vaccines and Diagnostics srl CQ Bioprocess support unit 53018 Rosia (SI), Italy
[^]Current address: IRBM Promidis, Via Pontina Km 30.600, 00040 Pomezia (Rome, Italy)

Conflict of interest

The authors declare competing financial interests: Alessia Tarditi, Eduardo Gonzalez-Couto, Giulia Lazzeroni, Freddy Heitz, Daniela Diamanti, Luisa Massai, Giuseppe Pollio, Guido Marconi, Chiara Caramelli, Arianna Nencini, Matteo Andreini, Gian Luca Sardone, Nicola P. Caradonna, Valentina Porcari, Carla Scali and Andrea Caricasole were employed by Siena Biotech; Michael Hannus and Birte Sönnichsen were employed by Cenix BioScience GmbH.

Europe PMC Funders Author Manuscripts

Huntington's disease (HD) is a currently incurable neurodegenerative condition caused by an abnormally expanded polyglutamine tract in huntingtin (HTT). We identified novel modifiers of mutant HTT toxicity by performing a large-scale "druggable genome" siRNA screen in human cultured cells, followed by hit validation in *Drosophila*. We focused on glutaminyl cyclase (QPCT), which had one of the strongest effects on mutant HTT-induced toxicity and aggregation in the cell-based siRNA screen, and which also rescued these phenotypes in *Drosophila*. We found that QPCT inhibition induced the levels of the molecular chaperone alpha B-crystallin and reduced the aggregation of diverse proteins. We generated novel QPCT inhibitors using *in silico* methods followed by *in vitro* screens, which rescued the HD-related phenotypes in cell, *Drosophila* and zebrafish HD models. Our data reveal a novel HD druggable target affecting mutant huntingtin aggregation, and provide proof-of-principle for a discovery pipeline from druggable genome screen to drug development.

Introduction

Huntington's disease (HD) is a fatal, currently incurable, late-onset neurodegenerative disorder. The disease signs include involuntary and repetitive choreic movements, psychological dysfunction and cognitive impairment, which result from progressive degeneration of cortical and striatal neurons [12].

HD is caused by the expansion of a CAG repeat tract in exon 1 of the gene encoding huntingtin (HTT), which results in an abnormally long polyglutamine stretch in the N-terminus of the protein [3]. Although the mechanisms are not fully understood, it is believed that the disease arises from a toxic-gain-of function of the mutant protein [45]. A hallmark of HD is the presence of intracellular aggregates, which is also a characteristic of the other ten polyglutamine-expansion disorders, as well as other neurodegenerative conditions such as Parkinson's or Alzheimer's disease [6]. The role of these aggregates in the disease is not clear, although an increasing importance of the oligomeric forms in toxicity is emerging [78] and reducing mutant HTT aggregation with strategies such as pharmacological upregulation of chaperone function has been pursued as a therapeutic strategy in HD [9]. Mutant HTT toxicity is believed to be accentuated, or possibly induced, after cleavage events resulting in the formation of short N-terminal polyglutamine containing fragments, which can also be produced by aberrant splicing [10]. Hence, exon 1 models have been frequently used for disease modeling.

Here, we combined two approaches to identify modifiers of mutant HTT toxicity by first performing a cell-based screen to identify genes that when knocked down could suppress mutant HTT-induced toxicity, using a library of 5,623 siRNAs selected according to the potential druggability of their targets with small molecules [11]. We performed this screen in two different HD models. Initially, we screened the effects of siRNAs in a mammalian cell line inducibly expressing HTT with an abnormal polyglutamine expansion. In a secondary analysis, we validated primary hits in a *Drosophila* model of HD.

One of the strongest suppressors of mutant HTT toxicity in both mammalian cells and *Drosophila* was an enzyme responsible for the modification of N-terminal residues of glutamine or glutamate into an N-terminal 5-oxoproline or pyroglutamate (pE), named

Europe PMC Funders Author Manuscripts

glutaminyl cyclase (QPCT).. QPCT not only suppressed mutant HTT induced toxicity but also greatly reduced the number of aggregates. This effect is not HTT-specific, since QPCT exerted a general effect on aggregation of different aggregate-prone proteins, including other proteins containing an expanded polyglutamine or polyalanine tract, which could be attributed to increased levels of the chaperone alpha B-crystallin upon QPCT inhibition. Furthermore, we designed small molecule modulators of QPCT activity, which effectively suppressed mutant HTT aggregation and toxicity in cells, neurons, fly and zebrafish models of the disease.

Results

Primary cell screen for suppressors of mutant Htt toxicity

We performed the primary screen using a stable HEK293/T Rex cell line expressing full-length human HTT bearing 138 polyglutamines (Q138) under the control of a tetracycline-inducible promoter. We confirmed the expression of HTT(Q138) after inducing the cells with doxycycline using antibodies recognizing the N-terminus of human HTT (Supplementary Results, Supplementary Fig. 1a and Supplementary Note 1), and quantitative RT-PCR using primers spanning different areas of the human *HTT* cDNA (Supplementary Fig. 1b). This cell line had reduced cell viability after expression of mutant HTT, which was reverted by treatment with a known reference compound (Y27632) [12] (Supplementary Fig. 1c), suggesting that this model could be used to identify potential modulators of mutant HTT cellular toxicity in a large-scale screen.

For our high-throughput screen, we utilised a strategy consisting of an iterative siRNA screen where positive genes were selected after three consecutive rounds to compensate for the variability of the assay. We eliminated non-positive siRNAs and added new siRNAs targeting the selected genes in consecutive passes. We assessed rescue of cellular toxicity by each siRNA by fluorescence microscopy and automated image analysis using three independent readouts: 1) number of cell nuclei (#nuclei), 2) apoptotic index and 3) aberrant nuclei index, and used rescue indices to express the effect of each individual siRNA for each parameter analysed. In an initial screen, we tested 3 independent siRNAs for each of the 5,623 genes (a total of 16,869 siRNAs), from which we selected 670 primary genes (see Supplementary Note 1 for screen assay and criteria selection). As shown in supplementary figure 2a, the three readouts were partially redundant, as more than 50% of the 1,000 top scoring siRNAs of one rescue index also ranked amongst the top 1,000 siRNAs of at least one of the other rescue indices. In supplementary figure 1b, a representation of rescue indices obtained in pass 1 shows the relatively large variability of the assay, with non-targeting negative control siRNAs, negQ and negF, showing a #nuclei rescue indices of 14% and 3% respectively, while using siRNA targeting HTT as a positive control rendered a mean #nuclei rescue index of 81%.

After 3 consecutive rounds of screening, we selected and 257 genes and ranked these based on all three rescue indices, using #nuclei rescue index as a primary criterion (Supplementary Data Set 1).

Europe PMC Funders Author Manuscripts

Secondary RNAi screening in a *Drosophila* model of HD

To validate the hits obtained in mammalian cells and to focus on targets with potential relevance *in vivo*, we performed a secondary screen in a *Drosophila* model that expressed a construct containing 48 polyglutamines, Q48, that causes eye degeneration when expressed using a *GMR-GAL4* driver [13]. For most genes selected, we studied two UAS-RNAi constructs from the Vienna *Drosophila* RNAi Center (VDRC): a *P*-element (GD) and a *phiC31* (KK) construct, the latter of which carries more GAL4-binding sites and should therefore express the RNAi more strongly [14]. Of the 257 mammalian genes previously selected, we detected 133 that had one or more gene orthologs in flies (Supplementary Data Set 1 and 2). Of these 133 mammalian genes with fly orthologs, 74 *Drosophila* genes (corresponding to 66 mammalian genes) rescued the Q48-induced eye degeneration with at least one RNAi line, while the others showed no obvious or significant effect (Supplementary Fig. 3a and 3b and Supplementary Data Sets 1 and 2). We crossed suppressor RNAi lines to transgenic flies that expressed EGFP, also driven by the same *GMR-GAL4* driver. We used EGFP to test whether modifiers affected transgene protein synthesis, since Q48 levels can be modified by aggregation or autophagic degradation, which do not impact EGFP levels. Two of these fly RNAi lines, targeting orthologs to human CTSF and to human ADAM8, ADAM11 and ADAM33, reduced EGFP levels on western blots (Supplementary Data Set 2), suggesting a general effect of these genes in protein expression, while suppression exerted by the other RNAi lines seemed to be polyglutamine-specific.

Functional categorization of mutant HTT modifiers

To gain further insight into the biological relevance of the data generated, we categorized the different sets of HD toxicity modulators according to their molecular function. Suppressors were enriched for certain classes of proteins such as GPCRs or transporters compared to the initial library, while the number of positive kinases in the screen was reduced and no cytokines, growth factors or translational regulators were represented. We observed similar functional categorizations after selection from the cell and *Drosophila* screen (Supplementary Fig. 4a). An Ingenuity Pathway Analysis (IPA) of the hits obtained in the primary screen in cells (Supplementary Table 1a) revealed that the majority of these proteins participate in general processes such as GPCR- or cAMP-mediated signalling, but also in canonical pathways related to neurodegeneration, such as apoptosis, mitochondrial dysfunction, amyloid processing or protein ubiquitination. Importantly, 10 of these proteins have been previously related to HD signalling, including subunits of the succinate dehydrogenase complex and huntingtin-associated protein 1 (HAP1) (Supplementary Table 1a). Many of the genes validated in *Drosophila* (Supplementary Fig. 4b and Supplementary Table 1b) are also involved in processes related to neurodegeneration but were enriched in mitochondrial metabolic pathways, especially those associated with fatty acid biosynthesis and metabolism.

Validation of QPCT in *Drosophila*

We focused our attention on a gene that had one of the strongest and most consistent effects in rescuing mutant HTT-induced toxicity in the cell-based siRNA screen. The gene product

has glutaminyl cyclase activity and is named QPCT. Two orthologs have been reported in fly [15], *Glutaminyl cyclase* (*QC*) and *iso Glutaminyl cyclase (isoQC*), which show about 39% amino acid identity; a third fly ortholog, CG6168, shows expression restricted to male accessory glands (www.flyatlas.org) and is not considered further here. RNAi lines targeting either *QC* or *isoQC* partially rescued eye depigmentation and mediated a significant decrease in the number of black spots in flies expressing Q48 (Fig. 1a, 1b and Supplementary Fig. 5a) (Data are shown for GD- and KK-RNAi lines in the case of *QC*, but only a KK line was available for *isoQC*). These effects are likely independent of transcription/translation of the Q48, since no change in EGFP protein levels were seen when we crossed transgenic flies expressing EGFP driven by the same *GMR-GAL4* driver as Q48 with *QC* or *isoQC* RNAi lines (Supplementary Fig. 5b). Thus, QPCT represents an interesting candidate for studying in HD.

To further evaluate the benefits of downregulating QPCT on HD, we took advantage of an additional *Drosophila* model of neurodegeneration, HD flies that express exon 1 of HTT with 120 polyglutamines, *GMR-HTT.Q120* in eye photoreceptors [16]. *Drosophila melanogaste*r has a compound eye consisting of many ommatidia, each of which is composed of 8 photoreceptors, seven of which can be visualized by light microscopy using the pseudopupil technique [17]. Neurodegeneration results in the loss of visible rhabdomeres of each photoreceptor and can be rescued or enhanced by genetic or chemical approaches [18]. Consistent with our data using the Q48 flies, the loss of visible photoreceptors in transgenic flies expressing *GMR-HTT.Q120* was partially rescued when they were crossed with RNAi lines for either of the two QPCT fly orthologues, *QC* and *isoQC* (Fig. 1c). We observed no effect on the number of rhabdomeres in QPCT RNAi lines in the absence of *GMR-HTT.Q120*. The effects of QPCT knockdown on toxicity correlated with a reduction in HTT aggregation, which we assessed in flies expressing GFP-tagged expanded huntingtin exon 1, *HTTEx1-Q46-eGFP* in the eye [19] (Fig. 1d).

QPCT modulates mutant HTT aggregation

To further validate QPCT, we first confirmed the protective effect of its knockdown against toxicity and aggregation in HEK293 cells expressing the exon 1 of *HTT* (from residue 8) with a 74 polyglutamine expansion fused at its N-terminal to EGFP (*EGFP-HTT(Q74)*) [20] (Fig. 2a, Supplementary fig. 6a and 6b). The QPCT siRNAs used in these experiments as well as in the screen do not target QPCT-like, which encodes a paralogous protein that catalyzes a similar reaction and shows 51% of sequence identity to QPCT (Supplementary Fig. 6b and 6c). We also validated the effect of QPCT knockdown on aggregation in HeLa cells (Supplementary Fig. 6d) which, like HEK293 cells, express QPCT [21]. We also confirmed a decrease in protein aggregation of a construct which expresses full-length HTT carrying 138 polyglutamines (similar to the one used in the initial screen) (Supplementary Fig. 6e). QPCT siRNA did not have a general anti-apoptotic effect as it did not affect caspase 3 activity in response to staurosporine treatment (Supplementary Fig. 6f). Consistent with these data, QPCT shRNA reduced EGFP-Q80 (80 glutamines fused to EGFP) aggregation in primary cortical neurons (Fig. 2b and Supplementary fig. 6g). We could not assess the effect of QPCT knockdown on polyglutamine-mediated toxicity in these neurons, where the levels of cell death obtained in this assay were very low, as can be appreciated in

fig. 2b. While knocking down QPCT was protective, overexpression of QPCT in HeLa and HEK293 cells increased the numbers of apoptotic nuclei and also led to a large accumulation of HTT(Q74) aggregates (Fig. 2c and Supplementary Fig. 7a), while QPCT did not increase caspase activity upon staurosporine treatment (Supplementary Fig. 7b). The effects of QPCT were activity-dependent, since the catalytically inactive E201Q mutant did not increase the percentage of cells with HTT(Q74) aggregates (Fig. 2d and Supplementary Fig. 7c and 7d).

We measured mRNA levels of QPCT in HD mice and found that its expression was reduced when compared to their wild-type littermates, suggesting that QPCT expression may be downregulated as a compensatory mechanism (Supplementary Fig. 8) and that raised QPCT activity may not be a prerequisite for aggregation.

QPCT catalyzes the modification of N-terminal glutamines or glutamates into a pyroglutamate (pE) residue. Although the presence of an extended polyglutamine tract makes HTT a potential substrate for QPCT, this enzyme only modifies N-terminal residues, suggesting that any modification on mutant HTT would require an N-terminal cleavage to reveal a glutamine at the N-terminal that could be cyclated. The formation of a pE residue may then affect its stability and propensity to aggregate, a hypothesis that was previously suggested [22]. This cleavage model in either the polyglutamine tract or HTT exon 1 or GFP is unlikely, as QPCT modulated the aggregation of constructs consisting only of isolated polyglutamine expansions (Q57 and Q81) fused C-terminal to EGFP (Fig. 2e and 2f), or HTT exon 1 with 74 glutamines fused to HA [23] (Supplementary Fig. 9a and 9b), and QPCT siRNA also reduced the aggregation of an expansion of 37 alanines [24] (Fig. 2f). QPCT appeared to modulate the early stages of mutant HTT oligomerisation, since QPCT overexpression increased the amounts of Flag-tagged monomeric mutant HTT that were co-immunoprecipitated by GFP-tagged mutant HTT (Fig. 2g) [25]. Since QPCT did not interact with HTT directly by immunoprecipitation (e.g. Fig. 2g), its effect on HTT oligomer formation is likely mediated via intermediaries.

Design and characterization of compounds that inhibit QPCT

To target QPCT pharmacologically, we tested a previously described QPCT inhibitor [26], which did not rescue the HD phenotype in mammalian cells (Supplementary Fig. 10a and 10b). While this compound has been effective in Alzheimer disease (AD) models by reducing the formation of extracellular pE-Aβ, this may be due to extracellular QPCT inhibition [2127]. Thus, we reasoned that the failure of this compound was likely due to poor cell permeability. In order to generate novel QPCT inhibitors, we employed existing data on its structure and known inhibitors to generate three 3D pharmacophore models, two ligand-based and one structure-based (using the human QPCT X-Ray structure (PDB id: 2AFW)). We used these models, along with stringently applied CNS filters and a solubility model developed in-house, to select 10,000 compounds from both commercially available screening compounds and the SienaBiotech compound library. We screened these molecules in a functional assay assessing the conversion of the H-Glu-AMC fluorogenic substrate into pyroGlu-AMC, as previously described [28], and selected hits associated with predicted robust binding for the hit-to-lead phase. The optimization strategy was based on physicochemical

properties and ensemble docking model-driven approaches. The ensemble docking methodology [29,30] was chosen to take into account the flexibility of human QPCT catalytic site and was constructed using both X-Ray structures and protein conformations coming from a 100 ns molecular dynamic study of the human QPCT 2AFW X-Ray structure. The ensemble docking model was evolved during the project development. Initially, only 4 X-Ray structures were used (PDB ID: 2AFW, 2AFX, 2AFZ[31]), then a set of 16 protein conformations, selected by clustering of molecular dynamic simulations, were added to improve model accuracy. Recently, two more X-Ray structures were added to the model (3PBB[32] an 3SI0[33]). All the docking calculations were performed using CCDC Gold (versions 4 and 5)[34,35,36] along with an ad-hoc developed program to rank and select the best scored ligand docking pose from the pool of QPCT conformations. Along with the biochemical readouts used during this optimization, we included a range of *in vitro* ADME assays, including solubility measurements, a CNS membrane permeability assay (PAMPA-BBB) [37] and stability in the presence of human CYP3A4, a member of the cytochrome P450 mixed-function oxidase system, and a key enzyme involved in the metabolism of xenobiotics in humans.

We selected a series of compounds on the basis of these properties and validated their effects on mutant HTT aggregation and toxicity in cells expressing HTT(Q74)GFP, which led to the selection of three of them, SEN177 (**1**), SEN817 (**2**) and SEN180 (**3**) (Supplementary note 2, Fig. 3a, Supplementary Fig. 11a). Non-toxic concentrations of these compounds caused a dose-dependent reduction in the percentage of cells with aggregates, which correlated with a suppression of mutant HTT-induced apoptosis (Fig. 3b, 3c, 3d, 3d and Supplementary Fig. 11b). As seen with genetic knockdown experiments, pharmacologic inhibition of QPCT using these compounds also reduced aggregation of polyalanines (Fig. 3d) and did not affect protein levels, as assessed by measuring GFP levels by western blotting (Supplementary Fig. 11c) or by metabolic labeling of wild type HTT followed by detection of newly synthesized protein in the presence of SEN177 (Supplementary Fig. 11d). Importantly, the effect of these compounds was blocked when QPCT expression was suppressed by shRNA, confirming that they protect by a mechanism that requires QPCT inhibition (Fig 3e, Supplementary Fig. 11e and 11f). Thus, even though these compounds also inhibited QPCT-like (Supplementary Fig. 11a) and we cannot exclude the possibility that at least some of the effects observed may be mediated by this QPCT isoenzyme, their effects on aggregation were QPCT-dependent, as the shRNA used did not target QPCT-like. Consistent with these data, SEN177 greatly reduced the early stages of mutant HTT oligomerisation, as it decreased the amounts of GFP-tagged monomeric HTT that were co-immunoprecipitated by Flag-tagged HTT (Fig. 3f). The protective effect of these compounds was also confirmed in primary cortical neurons (Fig. 3g), with SEN177 and SEN817 significantly reducing the percentage of neurons with Q80 aggregates.

QPCT modulates the levels of alpha B-crystallin

The effects of QPCT inhibition on HTT aggregation appeared to be independent of effects on protein clearance pathways targeting mutant huntingtin (autophagy and the ubiquitin-proteasome system) (Supplementary Fig. 12), changes in mRNA or protein levels (Supplementary Fig. 13a and 13b), or secretion of the enzyme into the medium

(Supplementary Fig. 13c). QPCT is localized in the ER and secretory pathway and its knockdown, overexpression or inhibition seemed to have inconsistent and rather modest effects on different readouts of the ER stress response, measured by GRP78/BIP levels or phosphorylation of eIF2α, which did not correlate with its effect on aggregation (Supplementary Fig. 14). Our data also suggested that CREB (c-AMP response element binding protein) or ERK (extracellular signal-regulated kinase) signaling, recently reported to be activated upon QPCT inhibition [38] (Supplementary Fig. 15a and 15b), or JNK signaling (Supplementary Fig. 15c) were unlikely contributors to the effects we have observed.

QPCT overexpression or knockdown did not modulate levels of HSP70, the main inducible stress response chaperone (Supplementary Fig. 15d). We performed transcriptional profiling to assess changes in alternative molecular chaperones induced by SEN177 in the presence of mutant HTT, and observed upregulation of several small heat shock proteins (sHSPs) (HSPB6 with 1.6 fold-change; HSPB3 with 1.5 fold-change; HSPB7 with 1.5 fold-change; and notably, alpha B-crystallin which had >2.5 fold increase in transcript levels) (Supplementary Fig. 16a and Supplementary Data Set 3). We confirmed this induction at the protein level as well as with other QPCT inhibitors (Fig. 4a). Genetic inhibition of QPCT dramatically increased alpha B-crystallin protein and mRNA levels in the presence of HTT(Q74) (Fig. 4b and 4c and Supplementary Fig. 16b), while QPCT overexpression, which increased mutant HTT aggregation and toxicity (Fig. 2c and Supplementary Fig. 7a), reduced alpha B-crystallin levels (Supplementary Fig. 16c). QPCT also modestly modulated alpha B-crystallin levels in the absence of mutant HTT or in the presence of the non-pathogenic Q23 (Supplementary Fig. 16b and 16c).

As a sHSP, alpha B-crystallin acts as a molecular chaperone and is a suppressor of polyglutamine toxicity in cells and in *Drosophila* [394041]. As expected, overexpression of alpha B-crystallin lowered the number of HTT(Q74) aggregates, while QPCT inhibitors failed to reduce aggregation further (Fig. 4d and Supplementary Fig. 16d), suggesting that this increment in alpha B-crystallin was a major contributor to the protection afforded by QPCT inhibition.

QPCT inhibition protects fly and zebrafish HD models

We tested QPCT inhibitors in flies expressing Httex1Q46 in the eye and found a reduction in the number of aggregates (Fig. 5a). The compound with a greatest effect, SEN177, was able to also rescue the number of visible rhabdomeres and prevent neurodegeneration (Fig. 5b).

A transgenic zebrafish expressing Htt exon 1 with 71Q fused to EGFP in the rod photoreceptors using the rhodopsin promoter has been established and validated as a model to study mutant huntingtin aggregation in vivo [42]. Zebrafish have two homologs with putative glutaminyl-peptide cyclotransferase activity, QPCT and QPCTLA with 51% and 47% protein identity with QPCT and QPCT-like respectively. In order to test the effect of pharmacologic inhibition of QPCT in this model, we first determined the maximum tolerated concentration for each of the three compounds tested in mammalian cells and subsequently treated HD larvae. SEN817 and SEN180 reduced total number of EGFP-

aggregates in the retina (Fig. 6a), which correlated with a marked decrease in toxicity similar to the positive control, clonidine [42], assessed by a rescue in the total area of eye photoreceptors (Fig. 6b).

Although the three compounds were protective, their effectiveness varied between these models, which might be due to intrinsic properties of each system, SEN180 only mildly reduced aggregation in neurons and the effect of SEN817 was not significant in *Drosophila*. Although SEN177 had the highest *in vitro* activity and was able to efficiently reduce aggregates in mammalian cells, primary neurons and *Drosophila*, we found that this compound was tolerated at much higher concentrations than its analogs in zebrafish and therefore the bioavailability in this model is much lower, which could explain the lack of effect in this system. All together, we have identified a number of small molecules that through QPCT inhibition have beneficial effects on the treatment of HD in a variety of *in vivo* models.

Discussion

Our approach using a two-step screen, starting with an initial large-scale analysis in human cell models followed by a validation in *Drosophila*, has yielded a number of potentially druggable targets which may be suitable for HD. A variety of HT-RNAi screens have identified genetic suppressors of phenotypes mediated by mutant HTT N-terminal fragments in *Drosophila*, *C. elegans* and mammalian (mouse and human) cells [44454647]. In most cases, aggregation was the primary readout, often measured with C-terminal GFP fusions. Differences in the nature of the previous screens (species, cellular context, huntingtin fragment length, length of the polyglutamine expansion, primary readout and differences in siRNA/shRNA sequences) complicates cross-screen comparisons. Also, virtually no screens in this area have examined their false negative rates due to inefficient knockdown. Additionally, the screen presented here was biased towards the druggable component of the human genome, and a further selection was made in the course of triaging towards specific protein target classes. This likely contributes to the relatively poor overlap of hits in the present and previous screens. A comparison with a screen performed in HEK293T cells to identify genetic suppressors of inducibly expressed mutant HTT exon 1 toxicity [46] revealed an overlap of only 4 genes (CPA1, GRIN2A, NR3C2 and USP21) when considering the top 257 hits (Supplementary Data Set 1). However, matrix metalloproteases, identified in HEK293T cells as modulators of fragmentation and toxicity of N-terminal portions of mutant HTT [45] were also identified in our dataset, as well as PAK1, which we previously identified as a kinase promoting mutant HTT self-association and toxicity [25], thus validating the effectiveness of the screen.

Based on the reproducible and clear rescue that QPCT inhibition exerts on mutant HTT toxicity in cells and in *Drosophila*, we focused on this target. A catalytically inactive QPCT was not able to increase the number of aggregates, suggesting that pE modifications modulate the levels of aggregates in HD models. Although one obvious mechanism would involve cleavage of the polyglutamine tract followed by cyclation of an N-terminal pE residue that may change properties such as stability or hydrophobicity, which would account for its change in aggregation [22], our data suggest that the effect of QPCT on HTT may be

indirect. We found that modulation of aggregation by QPCT was not restricted to mutant HTT but it also affected aggregation of other aggregate-prone proteins and that QPCT influences the formation of mutant HTT oligomeric species. We observed an induction in several sHSPs, mostly alpha B-crystallin, suggesting that QPCT inhibition caused a stress response distinct from classical Hsp70 induction, which might be mediated by indirect substrates for pE modification. This molecular chaperone reduces aggregation of polyglutamine containing proteins [3941], alpha-synuclein [4841]or amyloid-β peptide [4950], underscoring QPCT inhibition as an effective target for misfolded protein disorders. Since alpha B-crystallin is regulated at the transcriptional level while QPCT resides in the secretory pathway, inhibition of QPCT may activate a signalling response that enhance alpha B-crystallin transcription. Our data suggest that this is likely independent of an ER stress response or the involvement of ERK and CREB, which have been recently found phosphorylated upon QPCT inhibition [38], as well as other stress signalling pathways such as JNK. Further work will need to clarify the QPCT substrate mediating this effect. It is important to stress that the benefits of QPCT downregulation may not be restricted to alpha B-crystallin as an effector, as the upregulation of other related sHSPs may also contribute beneficially.

We identified and characterised a series of compounds that efficiently reduce mutant HTT aggregation in mammalian cell lines and also in primary mouse neurons, fly eye and in zebrafish. While the levels of rescue and significance obtained varied between compounds depending on the model used, this may be as a result of differences in absorption routes and bioavailability. Nevertheless, our data showed that pharmacologic inhibition of QPCT using this compound series can rescue HD phenotypes and provides proof-of-principle for QPCT as a potential therapeutic target for HD and possibly other related intracellular proteinopathies by modulating the formation of oligomeric forms, which have been proposed as the most toxic species in these diseases [78]. Clearly, further work is required before considering that this will be clinically relevant, including likely additional drug development. Nevertheless, in a broader perspective, our data suggest that a discovery pipeline from druggable genome screen to drug development may be tractable for neurodegenerative diseases.

Online Methods

Assays for validation polyglutamine toxicity modifiers in *Drosophila*

***Drosophila* fly stocks—**As a model of polyglutamine toxicity, flies that expressed a protein with 48 glutamines encoded by *P{UAS-Q48.myc/flag}31* [13] in eyes under control of the GMR-Gal4 driver *P{GAL4-ninaE.GMR}12* [51] (Q48) were used. Fly orthologs to the genes identified in the cell screen were selected by performing reciprocal BLASTP and cross checking with databases including http://www.ncbi.nlm.nih.gov/homologene, http://www.genecards.org/, http://www.ensembl.org/index.html. The RNAi lines corresponding to the identified genes were obtained from Vienna *Drosophila* RNAi Center (VDRC, http://stockcenter.vdrc.at/control/main).

Europe PMC Funders Author Manuscripts

The following stocks were generous gifts: *UAS-Q48.myc/flag* from J.L. Marsh [13], *UAS-Httex1-Q46-eGFP* from N. Perrimon [19]. Fly lines that are not referenced here are documented in FlyBase (www.flybase.org).

All fly crosses and experiments were performed at 25°C.

***Drosophila* RNAi screen—**Five virgins of genotype *w; GMR-GAL4; UAS-Q48.myc/flag* (Q48) were crossed to males carrying each *UAS-RNAi* (GD- and KK-RNAi collections, VDRC, http://stockcenter.vdrc.at/control/main). Genetic background was controlled by crossing *w; GMR-GAL4; UAS-Q48.myc/flag* females to w^{1118} males that share the same genetic background (VDRC stock number 60000 for the GD-RNAi lines and 60100 for the KK-RNAi lines). For *Glutaminyl cyclase* (CG32412) the GD-RNAi line 38277 and the KK-RNAi line 106341 were used. For *isoGlutaminyl cyclase* (CG5976), the KK-RNAi line 101533 was used. For GD-RNAi lines, degeneration was determined by scoring the eye depigmentation in the progeny of the above crosses 4 days after eclosion, assessing modification of polyglutamine loss-of-pigmentation and black necrotic-like spots. For KK-RNAi lines, as their background leads to dark eye pigmentation (http://www.vdrc.at/rnai-library/rnai-protocols), toxicity was assessed by scoring the presence or abscence of black necrotic-like spots in the eyes of 10-day old flies. Fisher's exact test was performed to compare the numbers of necrotic-spot-containing flies in the KK-RNAi crosses with controls using an arbitrary $p<0.005$ as a statistical cut-off for significance. Eyes were imaged using a Nikon CoolPix 990 digital camera attached to a dissecting microscope.

EGFP expression levels assessed in Drosophila RNAi lines—Western blot analysis was performed using progeny of crosses between virgins of the genotype *w; GMR-GAL4; UASEGFP* and males of each VDRC-RNAi line used or background control (VDRC stock number 60100). Fly heads were homogenized in Laemmli sample buffer. Rabbit polyclonal anti-GFP at 1:1000 (AbCam, Ab6556) and monoclonal anti-beta tubulin at 1:10000 (Developmental Studies Hybridoma Bank) were used. Blots were scanned using Odyssey Fc Imaging System (LI-COR Biosciences). This validation was initially performed once on each suppressor, and subsequently RNAi lines showing an apparent reduction in EGFP levels were re-tested using the progeny of three independent crosses. Statistical analysis was performed by two-tailed paired t-test between the RNAi lines and the control line.

Pseudopupil assay—Analysis was performed as previously described [17]. Virgins of genotype *elav-GAL4*^{C155}; *{GMR-HD.Q120}4.62/TM3* (elav-Gal4; GMR-HTT.Q120) [16] were crossed with males carrying the RNAi construct for *Glutaminyl cyclase* (lines $QC^{GD38277}$ or $QC^{KK106341}$) or *isoGlutaminyl cyclase* (line $isoQC^{KK101533}$) and compared to background control line.

To evaluate the effect of QPCT inhibitors, virgins of genotype *yw*; {*GMRHD.Q120}2.4* (GMR-HTT.Q120) were allowed to mate with w^{1118} control males for 48 hours on standard cornmeal food and then transferred on fly food containing the compounds.

Europe PMC Funders Author Manuscripts

The number of rhabdomeres per ommatidium was scored in progeny of the above crosses at 3 (GMR-Q120) or 4 (elav-Gal4; GMR-HTT.Q120) days post-eclosion. Statistical analysis was performed using one-tailed t-test on data from 3 or 4 independent experiments, each based on approximately 10 individuals for each genotype, scoring 15 ommatidia per eye. When compounds were tested, the analysis was done on females and males of each treatment separately.

Aggregate counting—Virgins of genotype *w; GMR-GAL4; UAS-Httex1-Q46-eGFP* [19] were crossed with males of QPCT *UAS-RNAi* lines or from the background KK-RNAi control line, since all the background controls show similar aggregate scoring. Eye pictures of 18-day old progeny were taken using a Leica MZ16F microscope connected to a Leica DFC340FX digital camera. For each genotype, GFP punctae indicating aggregate formation was counted using ImageJ "Cell Counter" plugin in the eyes of 20 males, a pool of 5 males from four independent crosses. For compound testing, virgins of genotype *w; GMR-GAL4; UAS-Httex1-Q46-eGFP* were crossed with w^{1118} control males, and females of the progeny scored 15 days post-eclosion. The experiment was repeated at least three times and for each experiment at least 4 female eyes were scored. An unpaired one-tailed t-test was used to determine statistical significance for single comparisons between two groups using GraphPad Prism.

Compound treatment—Flies were reared on food (Instant Fly Food, Philip Harris, Ashby de la Zouch, UK) containing either QPCT inhibitor (50 μM) dissolved in DMSO or DMSO alone. The progeny were flipped every 2 days on fresh food containing the specific inhibitor or DMSO.

Bioinformatics Analysis

Ingenuity Pathways Analysis (Ingenuity® Systems, www.ingenuity.com) was used to analyze the distribution of siRNAs tested among the different protein classes as well as to determine the canonical pathways associated to the confirmed primary actives.

Assays for validation of polyglutamine toxicity and aggregation modifiers in human cell lines

Cell culture—HEK293 (Human Embryonic Kidney), HeLa (Human cervical carcinoma) cells and Atg5-deficient (Atg5-/-) mouse embryonic fibrolasts (MEFs) (gift from N. Mizushima) were grown in Dulbecco's modified eagle medium supplemented with 10% FBS, 100 U/ml penicillin/streptomycin and 2 mM l-glutamine at 37°C in 5% CO_2. UbG76V-GFP-expressing stable HeLa cell line (kind gift from N.P. Dantuma) was maintained in medium containing 0.5 mg/ml G418.

Isolation and culture of mouse primary cortical neurons—Primary cortical neurons were isolated from C57BL/6 mice (Jackson Laboratories) embryos at E16.5. Briefly, brains were harvested and placed in ice-cold PBS/glucose where the meninges were removed and the cerebral cortices were dissected. After mechanical dissociation using sterile micropipette tips, dissociated neurons were resuspended in PBS/glucose and collected by centrifugation. Viable cells were seeded on poly-ornithine-coated 12-multiwell plates. Cells

were cultured in Neurobasal medium supplemented with 2 mM glutamine, 200 mM B27 supplement, and 1% Penicillin-Streptomycin at 37°C in a humidified incubator with 5% CO_2. One half of the culture medium was changed every two days until treatment. After 5 days of culturing *in vitro*, differentiated cortical neurons were infected with lentiviral particles bearing EGFP-Q80 and scramble or QPCT-directed shRNAs. Compounds were added 3 days after EGFP-Q80 viral infection and left for another 24h. When EGFP-Q80 was expressed together with shRNA, 5-6 days were needed before cultures were fixed in a 2% PFA-7.5% glucose solution.

DNA constructs—Human QPCT (NM_012413) plasmid was purchased from Origene (*pCMV6-XL5-QPCT*). A C-terminal Flag-tagged QPCT construct was generated by PCR amplification of *QPCT* cDNA from *pCMV6-XL5-QPCT* using primers overhanging HindIII and BgIII sites and insertion into the pCMV5-FLAG in HindIII and BamHI restriction sites, using standard restriction enzyme digestion and ligation procedures. *QPCT(E201Q)-Flag* was generated using QuickChange II Agilent Site-Directed mutagenesis kit with the following primers Fw 5′-CTTCTTTGATGGTCAAGAGGCTTTTCTTCACTGG-3′ and Rev 5′-CCAGTGAAGAAAA GCCTCTTGACCATCAAAGAAG-3'. *pcDNA* or *pCMV5-Flag* empty vectors were used as mock controls for *pCMV6-XL5-QPCT* or *QPCT-Flag* respectively.

Constructs expressing the first exon of the Htt gene carrying 74 polyglutamines expressed from *pEGFP-C1* (Clontech) (*EGFP-HTTQ74*) or pHM6 (Roche Diagnostics) (*HAHTTQ74*), or with only 23 polyglutamines (*EGFP-HTTQ23*), were described previously [52]. *pEGFP-N1-Q57* and *pEGFP-N1-Q81* [23] and *pEGFP-C1-A37* [24] have been previously described. Mutant *HTT(1-588)-Flag* was provided by MR Hayden and mutant *HTT(1-548)GFP* generated by S. Luo [25]. 3xFlag-CRYAB construct has been previously described [53]. The pGL3-BIP/GRP78-luciferase construct was kindly provided by M. Renna [54]

Reagents—Chemical compounds used in cell culture were the autophagy inhibitors Bafilomycin A1 (400nM, DMSO; 4 hours; Millipore) and 3MA (10 mM, 16 hours; SIGMA), staurosporine (3 μM) and the proteasome inhibitor MG132 (10 μM). PBD150 was synthesized as described in [26].

Transfection—Cells were transfected in 6-well plates with 0.5-1.5 μg of DNA and 5 μl of Lipofectamine (Invitrogen) or TransIT-2020 (Mirus) per well for 4 hours in Optimem (GIBCO-BRL) and then incubated in full media for 48 hours. Gene knockdown experiments were performed using ON-TARGETplus SMARTpool siRNA (Dharmacon) for human QPCT, consisting on 4 siRNAs with the following sequences: CUAUGGGUCUCGACACUUA; GUACCGGUCUUUCUCAAAU; CCUUAAAGACUGUUUCAGA; GGAACUUGCUCGUGCCUUA, and which do not target the QPCT like sequence. For siRNA treatment, a single transfection protocol using 50nM siRNA for 48 h or a double transfection protocol which consisted on a first 50 nM siRNA transfection followed by a second 50 nM siRNA transfection after 48 hours.

Western blotting—Cells were washed once in PBS and harvested on lysis buffer (20 mM Tris-HCl pH 6.8, 137nM NaCl, 1 mM EGTA, 1% Triton X-100, 10% glycerol, 1x Roche

complete mini protease inhibitor). Equal loading was obtained by protein concentration determination using a Bio-Rad assay followed by resuspension and boiling in Laemli buffer. Samples were subjected to 12% SDS-PAGE and transferred to PVDF membrane (Immobilion-P, GE Healthcare). Blots were proved with primary antibody: anti-LC3 (1:2000; Novus Biologicals, NB100-2220), anti-Hsp70 (1:1000; Enzo SPA810), anti-CRYAB (1:1000; Cell signalling 8851), anti-actin (1:2000; Sigma, A2066), anti-α-tubulin (1:4000; T9026, Sigma), anti-Flag epitope (1:2000; SIGMA, F7425), anti-GFP (1:1000; Clontech, Living colours, polyclonal), eIF2α (1:1000, Abcam 5369) and phospho-S51-eIF2α_(1:1000, Abcam 32157), GRP78 (1:1000, Abcam 21685), anti-phospho-ERK (1:1000, Cell signalling, 9101), anti-ERK (1:1000, Cell signalling, 9102), anti-phospho-CREB (S133) (1:1000, Cell signalling 9191), anti-CREB 86B10 (1:1000, Cell signalling, 9104), anti-phospho-JNK (1:1000, Cell signalling, 9255), anti-JNK (1:1000, Cell signalling, 9252). The appropriate anti-mouse or anti-rabbit secondary antibodies were used and visualized using an ECL detection kit (Amersham) or LI-COR Biosciences infrared imager (Odyssey).

Caspase 3/7 activity assay—Cells were seeded in a 96-well plate 24h prior to the assay and 1 μM staurosporine or DMSO was added for the last 8h. Caspase 3/7 activity was measured by using a luminogenic caspase 3/7 substrate (Caspase 3/7-Glo Assay, Promega) following manufacturer protocols in a Glomax luminometer (Promega). Protein concentration was determined in each cell lysate and caspase 3/7 activity was normalized to protein levels.

Co-inmunoprecipitation assays—Assays were performed as previously described [25], where HTT(1-588)Flag(Q138) and HTT(1-548)GFP(Q138) were expressed in HeLa cells together with QPCT plasmid for 48h, or treated with 25 μM SEN177 for 24h. Cells were lysed in buffer B containing 10 mM Tris pH 7.4, 150 mM NaCl, 1 mM EDTA pH8, 1% triton and 1x Roche complete mini protease inhibitor for 20 min on ice, followed by centrifugation at 13000 rpm for 10 min. Five hundred micrograms total protein were incubated with primary anti-Flag M2 (Sigma) or anti-GFP (Clontech, Living colours, polyclonal) at 5 μg/ml overnight at 4°C. Protein G Dynabeads (LifeTechnologies) were added and incubated for further 2 h. Beads were washed 3 times with buffer B and eluted using 0.1 M glycine pH 2.5M followed by boiling in laemli buffer. Samples were subjected to western blot and visualized using LICOR. A fraction of the total lysates was run simultaneously.

Reverse-transcriptase PCR analysis—Total RNA was isolated from cell pellets using Trizol Reagent (Invitrogen), treated with DNase I, and cDNA synthesis was performed by SuperScript III First-Strand Synthesis System (Invitrogen). Standard conditions were used for cDNA amplification and PCR products were analyzed by agarose gel electrophoresis and ethidium bromide staining or quantitated with real-time PCR. For real-time PCR analysis, the reaction mixture containing cDNA template, primers, and SYBR Green PCR Master Mix (Invitrogen) was run in a 7900 Fast Real-time PCR System (Applied Bio-systems, Carlsbad, CA). Fold changes on mRNA levels were determined by standard curve and after normalization to internal control β-actin RNA levels. Primer sequences used in this study

are: QPCT, 5′-CATGGCATGGATTTATTGG-3′ and 5′- GACGGTATCAGATCAAAC-3′; QPCT-like, 5′- CAGCGTCTCTGGAGCACTTA-3′ and 5′-GCCTCCAGGAACTTTCTGACT-3; GFP 5′- ACGTAAACGGCCACAAGTTC-3′ and 5′-TTCAGGGTCAGCTTGCCGTA-3′; actin, 5′-AGAAAATCTGGCCCACACC-3′ and 5′-GGGGTGTTGAAGGTCTCAAA-3′; CRYAB, 5′- TCTTGAGCTCAGTGAGTACTGG-3′ and 5′-AGCTCACCAGCAGTTCATGG-3′; and mouse QPCT, 5′-CGACTTGAGCCAATTGCTGA-3′ and 5′-CTTCCGGGTTAAGAGTGCTG-3′.

mRNA isolation from mouse brain—All mouse experiments were performed under appropriate UK Home Office licences and following institutional procedures. We analyzed samples from N171 mutant HD mice and wild-type littermate controls at 20 week. mRNA was extracted from brains homogenized in Trizol (Invitrogen) using an Ultra torax homogenizer.

Lentivirus infection—shRNA containing pLKO.1 vectors targeting both mouse and human QPCT (TRCN032432) were obtained from The RNAi Consortium (TRC) and scramble shRNA vector was generated in D. Sabatinit's laboratory (Addgene, plasmid 1864). Lentiviral plasmids to express Q80-GFP were kindly provided by J. Uney [55]. Lentiviral particles were produced and transduced following The RNAi Consortium protocols.

Cell toxicity and aggregation assays—Cells were fixed for 7 minutes in 4% paraformaldehyde (PFA). For EGFP-tagged constructs, slides were mounted in Citifluor (Citifluor, Ltd.) containing 4′,6-diamidino-2-phenylindole (DAPI; 3 μg/ml; Sigma) and visualized using an Eclipse E600 fluorescence microscope (plan-apo 60x/1.4 oil immersion lens) (Nikon). For detection of HA-tagged constructs, inmunofluorescence with an anti-HA (Covance laboratories 1:500) and anti-mouse Alexa488 secondary antibody (Invitrogen, 1:1000) was performed followed by mounting in Citiflour-DAPI. We assessed the percentage of transfected cells (EGFP- or HA-positive cells) with at least one aggregate per cell. Apoptotic cell death was determined by assessing the nuclear morphology (nuclei fragmented or condensed) in transfected cells. Slides were blinded and at least 200 transfected cells per slide were scored; each individual experiment was performed in triplicate.

Detection of nascent protein synthesis—Protein synthesis was assessed by metabolic incorporation of AHA (L-azidohomoalanine) into cells transfected with EGFP-HTT(Q23). Briefly, 12 hours after HeLa cells transfection, media was washed and replaced with L-methionine/L-cysteine free medium and treated with DMSO or SEN177 (50 uM) for 1h prior to addition of AHA (L-azidohomoalanine) to the media and collection of cells every 2 hours. Labelled protein was detected by western blot after performing Click-IT protein detection assay (Life Technologies) using biotin, following manufacturer protocols.

Luciferase reporter assay—Cells were transfected with 1 μg of GRP78-luciferase (*firefly*) reporter construct and 50 ng of *renilla*-luciferase (pRL-TK) as an internal transfection efficiency control. Cells were collected in Passive lysis buffer and luciferase activity was measured using the Dual-luciferase Reporter Assay System (Promega)

following manufacturer's protocol in a Glomax Luminometer (Promega). GRP78-luciferase relative activity was calculated relative to the *renilla*-luciferase transfection efficiency control activity for each sample; experiments were performed in triplicate.

Statistical analysis—Quantification of immunoblots was performed by densitometric analysis using the Image J software or the LI-COR Biosciences infrared imager software and normalized to loading control (actin or tubulin, as indicated). The *p*-values were determined by two-tailed Student's t-test.

Aggregates were counted in at least 200 cells per slide (with the observer blinded to their identity), and percentage was calculated relative to control conditions. *p*-values were determined by unpaired two-tailed Student's t-test.

All experiments were done at least three times in triplicate and a representative blot or graph from a triplicate experiment is shown unless indicated.

Heat shock proteins and chaperones PCR array—The Human Heat Shock Proteins and Chaperones RT2 Profiler PCR Array (SABiosciences, Frederick, MD) was used to study the expression profile of 84 heat shock proteins according to the manufacturer's procedure. Briefly, total RNA was extracted from cells transfected with HTT(Q74)GFP treated with DMSO or 25 uM of SEN177 inhibitor for 24h, using Trizol (Invitrogen) and further purified using RNeasy mini kit with oncolumn DNAse digest (Qiagen), cDNA was then synthesized using an RT2 First strand kit (SABiosciences) and real-time PCR was performed using 7900HT fast real time PCR system (Applied iosciences). Data were analysed with RT2 profiler PCR array data analysis software version 3.5.

Assays for validation of polyglutamine aggregation modifiers in zebrafish

Maintenance of zebrafish stocks and collection of embryos—All zebrafish husbandry and experiments were performed in accordance with UK legislation under a licence granted by the Home Office and with local ethical approval. Zebrafish were reared under standard conditions (Westerfield et al, 2005) on a 14 h light/10 h dark cycle. Embryos were collected from natural spawnings, staged according to the established criteria [56] and reared in embryo medium (5 mM NaCl, 0.17 mM KCl, 0.33 mM $CaCl_2$, 0.33 mM Mg_2SO_4, 5 mM HEPES).

Determination of the maximum-tolerated concentration of compounds in larval zebrafish—Compound exposure experiments were performed on wild-type larvae (TL strain) from 2 to 3 days post-fertilization (d.p.f.). Concentration response assays were performed over log intervals, from 100 nM to 1 mM, to determine the maximum non-toxic concentration (MTC) for subsequent aggregate analysis assays (n=10 larvae per concentration). Compound exposure experiments were performed in the dark at 28.5 °C.

Measuring aggregate number and rhodopsin protein levels in transgenic HD zebrafish—Aggregate counting and analysis of rod photoreceptor degeneration (photoreceptor number) was performed using heterozygous larvae from Tg (rho:EGFP-HTT71Q)^{cu5} zebrafish [42] (hereafter referred to as transgenic HD zebrafish). Embryos from

outcrossed transgenic HD zebrafish were raised in 0.2 mM 1-phenyl-2-thiourea (PTU) from 1 to 3 d.p.f. to inhibit pigment formation, screened for transgene expression using EGFP fluorescence, and then washed twice in the embryo medium to remove PTU. From 3 to 9 d.p.f., transgenic HD zebrafish larvae were dark-reared in embryo medium alone or embryo medium contain containing either DMSO, 1mM SEN177, 100 μM SEN180 or 100 μM SEN817. Embryo medium and compounds were replenished daily. Larvae were anaesthetized by immersion in 0.2 mg/ml 3-amino benzoic acid ethyl ester (MS222), then fixed for aggregate counting at 7 d.p.f. or for photoreceptor analysis at 9 d.p.f. Anaesthetised larvae were fixed using 4% paraformaldehyde (PFA) in PBS at 4 °C. Larvae were washed briefly in PBS, allowed to equilibrate in 30% sucrose in PBS then embedded in OCT medium (Tissue-Tek) and frozen on dry ice for subsequent cryosectioning. Sections were cut at 10 μm thickness using a cryostat (Bright Instruments). For aggregate counting, sections were mounted in 50% glycerol in PBS and the total number of GFP-positive aggregates were counted over 100 μm of the central retina, either side of the optic nerve head and mean values were calculated (n = 5 fish (10 eyes)) for each treatment group. For quantification of photoreceptor number, the GFP-positive area of the central retina was quantified using image thresholding and area analysis in ImageJ (n ≥ 5 fish (10 eyes) for each treatment group). To demonstrate that loss of GFP corresponds to loss of photoreceptors, sections were stained with anti-rhodopsin (1D1) antibody (a kind gift from Paul Linser, University of Florida, FL [57] and mounted using VectaShield hard set mounting medium (Vector Laboratories). Sections were viewed and representative images acquired using a GX Optical LED fluorescent microscope, GXCAM3.3 digital camera and GX Capture software.

Supplementary Material

Refer to Web version on PubMed Central for supplementary material.

Acknowledgements

We are grateful for funding from the MRC (COEN Grant MR/J006904/1 to DCR and CJO'K), the Wellcome Trust (Principal Fellowship to DCR; 095317/Z/11/Z), NIHR Biomedical Research Unit in Dementia at Addenbrooke's Hospital, the TAMAHUD project (European community's FP6 grant n.03472 under the Thematic Call LSH-2005-2.1.3-8 "Early markers and new targets for neurodegenerative diseases") and the NEUROMICS project (European community's Seventh Framework Programme under grant agreement No. 2012-305121). We thank J. L. Marsh, N. Perrimon, and the Vienna *Drosophila* RNAi Center for fly stocks, M. Renna and S. Luo for helpful comments, M Lichtenberg for help with flow cytometry assays, F. Siddiqi and M. Garcia-Arencibia for help with primary cultures, W. Fecke for advice and assistance and Stefano Gotta for help in HR-MS analysis of compounds.

Author Contributions

M.J.S. performed most post-screen cell biology experiments. W.L. and S.I. performed the Drosophila experiments. M.H. and B.S. performed the cell-based screen. A.F., T.E.D. and C.X performed the zebrafish experiments and A.F. supervised these. A.T., E.C.G. V.P.S. and R.S. performed the bioinformatics analyses. F.M. performed the chaperone transcription array experiments and non-radioactive pulse-chase. E.G.C. and F.H. participated in experimental design of the screen. F.H., G.L., D.D., L.M. and G.P. generated and validated the stable cell lines for the screen. G.M., C.C., A.N. synthesized and analyzed the compounds. M.A. performed the selection of compound for HTS and supported the hit to

Europe PMC Funders Author Manuscripts

lead optimization by in-silico drug design methodologies. V.P. optimized glutaminyl cyclase enzymatic assays for compound screening. G.L.S. and N.P.C. performed in vitro ADME experiments. C.S. provided support for experiments at Siena Biotech. C.O.K. supervised Drosophila experiments. G.P. also supervised molecular biology activities at Siena Biotech. A.C. supervised primary screen and chemical biology. D.C.R. supervised cell biology, Drosophila and zebrafish experiments. D.C.R and A.C. conceived the project and coordinated work between sites with assistance from G.P. M.J.S., D.C.R. and A.C drafted the manuscript which was commented on by all authors.

References

1. Imarisio S, et al. Huntington's disease: from pathology and genetics to potential therapies. Biochem. J. 2008; 412:191–209. [PubMed: 18466116]
2. Zuccato C, Valenza M, Cattaneo E. Molecular mechanisms and potential therapeutical targets in Huntington's disease. Physiol. Rev. 2010; 90:905–981. [PubMed: 20664076]
3. A novel gene containing a trinucleotide repeat that is expanded and unstable on Huntington's disease chromosomes. The Huntington's Disease Collaborative Research Group. Cell. 1993; 72:971–983. [PubMed: 8458085]
4. Mangiarini L, et al. Exon 1 of the HD gene with an expanded CAG repeat is sufficient to cause a progressive neurological phenotype in transgenic mice. Cell. 1996; 87:493–506. [PubMed: 8898202]
5. Hodgson JG, et al. A YAC mouse model for Huntington's disease with full-length mutant huntingtin, cytoplasmic toxicity, and selective striatal neurodegeneration. Neuron. 1999; 23:181–192. [PubMed: 10402204]
6. Soto C, Estrada LD. Protein misfolding and neurodegeneration. Arch. Neurol. 2008; 65:184–189. [PubMed: 18268186]
7. Takahashi T, et al. Soluble polyglutamine oligomers formed prior to inclusion body formation are cytotoxic. Hum. Mol. Genet. 2008; 17:345–356. [PubMed: 17947294]
8. Lajoie P, Snapp EL. Formation and toxicity of soluble polyglutamine oligomers in living cells. PloS One. 2010; 5:e15245. [PubMed: 21209946]
9. Hartl FU, Bracher A, Hayer-Hartl M. Molecular chaperones in protein folding and proteostasis. Nature. 2011; 475:324–332. [PubMed: 21776078]
10. Sathasivam K, et al. Aberrant splicing of HTT generates the pathogenic exon 1 protein in Huntington disease. Proc. Natl. Acad. Sci. U. S. A. 2013; 110:2366–2370. [PubMed: 23341618]
11. Bleicher KH, Böhm H-J, Müller K, Alanine AI. Hit and lead generation: beyond high-throughput screening. Nat. Rev. Drug Discov. 2003; 2:369–378. [PubMed: 12750740]
12. Li M, Huang Y, Ma AAK, Lin E, Diamond MI. Y-27632 improves rotarod performance and reduces huntingtin levels in R6/2 mice. Neurobiol. Dis. 2009; 36:413–420. [PubMed: 19591939]
13. Marsh JL, et al. Expanded polyglutamine peptides alone are intrinsically cytotoxic and cause neurodegeneration in Drosophila. Hum. Mol. Genet. 2000; 9:13–25. [PubMed: 10587574]
14. Dietzl G, et al. A genome-wide transgenic RNAi library for conditional gene inactivation in Drosophila. Nature. 2007; 448:151–156. [PubMed: 17625558]
15. Schilling S, et al. Isolation and characterization of glutaminyl cyclases from Drosophila: evidence for enzyme forms with different subcellular localization. Biochemistry. 2007; 46:10921–10930. [PubMed: 17722885]
16. Jackson GR, et al. Polyglutamine-expanded human huntingtin transgenes induce degeneration of Drosophila photoreceptor neurons. Neuron. 1998; 21:633–642. [PubMed: 9768849]
17. Franceschini N, Kirschfeld K. [Pseudopupil phenomena in the compound eye of drosophila]. Kybernetik. 1971; 9:159–182. [PubMed: 5134358]
18. Ravikumar B, et al. Dynein mutations impair autophagic clearance of aggregate-prone proteins. Nat. Genet. 2005; 37:771–776. [PubMed: 15980862]

19. Zhang S, Binari R, Zhou R, Perrimon N. A genomewide RNA interference screen for modifiers of aggregates formation by mutant Huntingtin in Drosophila. Genetics. 2010; 184:1165–1179. [PubMed: 20100940]
20. Wyttenbach A, et al. Effects of heat shock, heat shock protein 40 (HDJ-2), and proteasome inhibition on protein aggregation in cellular models of Huntington's disease. Proc. Natl. Acad. Sci. U. S. A. 2000; 97:2898–2903. [PubMed: 10717003]
21. Cynis H, et al. Inhibition of glutaminyl cyclase alters pyroglutamate formation in mammalian cells. Biochim. Biophys. Acta. 2006; 1764:1618–1625. [PubMed: 17005457]
22. Saido TC. Involvement of polyglutamine endolysis followed by pyroglutamate formation in the pathogenesis of triplet repeat/polyglutamine-expansion diseases. Med. Hypotheses. 2000; 54:427–429. [PubMed: 10783480]
23. Onodera O, et al. Oligomerization of expanded-polyglutamine domain fluorescent fusion proteins in cultured mammalian cells. Biochem. Biophys. Res. Commun. 1997; 238:599–605. [PubMed: 9299559]
24. Rankin J, Wyttenbach A, Rubinsztein DC. Intracellular green fluorescent protein-polyalanine aggregates are associated with cell death. Biochem. J. 2000; 348(Pt 1):15–19. [PubMed: 10794708]
25. Luo S, Mizuta H, Rubinsztein DC. p21-activated kinase 1 promotes soluble mutant huntingtin self-interaction and enhances toxicity. Hum. Mol. Genet. 2008; 17:895–905. [PubMed: 18065495]
26. Buchholz M, et al. The first potent inhibitors for human glutaminyl cyclase: synthesis and structure-activity relationship. J. Med. Chem. 2006; 49:664–677. [PubMed: 16420052]
27. Schilling S, et al. Glutaminyl cyclase inhibition attenuates pyroglutamate Abeta and Alzheimer's disease-like pathology. Nat. Med. 2008; 14:1106–1111. [PubMed: 18836460]
28. Schilling S, et al. Continuous spectrometric assays for glutaminyl cyclase activity. Anal. Biochem. 2002; 303:49–56. [PubMed: 11906150]
29. Yoon S, Welsh WJ. Identification of a minimal subset of receptor conformations for improved multiple conformation docking and two-step scoring. J. Chem. Inf. Comput. Sci. 2004; 44:88–96. [PubMed: 14741014]
30. Polgár T, Keserü GM. Ensemble docking into flexible active sites. Critical evaluation of FlexE against JNK-3 and beta-secretase. J. Chem. Inf. Model. 2006; 46:1795–1805. [PubMed: 16859311]
31. Huang K-F, Liu Y-L, Cheng W-J, Ko T-P, Wang AH-J. Crystal structures of human glutaminyl cyclase, an enzyme responsible for protein N-terminal pyroglutamate formation. Proc. Natl. Acad. Sci. U. S. A. 2005; 102:13117–13122. [PubMed: 16135565]
32. Huang K-F, et al. Structures of human Golgi-resident glutaminyl cyclase and its complexes with inhibitors reveal a large loop movement upon inhibitor binding. J. Biol. Chem. 2011; 286:12439–12449. [PubMed: 21288892]
33. Ruiz-Carrillo D, et al. Structures of glycosylated mammalian glutaminyl cyclases reveal conformational variability near the active center. Biochemistry (Mosc.). 2011; 50:6280–6288.
34. Jones G, Willett P, Glen RC. Molecular recognition of receptor sites using a genetic algorithm with a description of desolvation. J. Mol. Biol. 1995; 245:43–53. [PubMed: 7823319]
35. Jones G, Willett P, Glen RC, Leach AR, Taylor R. Development and validation of a genetic algorithm for flexible docking. J. Mol. Biol. 1997; 267:727–748. [PubMed: 9126849]
36. Verdonk ML, Cole JC, Hartshorn MJ, Murray CW, Taylor RD. Improved protein-ligand docking using GOLD. Proteins. 2003; 52:609–623. [PubMed: 12910460]
37. Palm K, Luthman K, Ros J, Grasjo J, Artursson P. Effect of molecular charge on intestinal epithelial drug transport: pH-dependent transport of cationic drugs. J. Pharmacol. Exp. Ther. 1999; 291:435–443. [PubMed: 10525056]
38. Song H, et al. Inhibition of Glutaminyl Cyclase Ameliorates Amyloid Pathology in an Animal Model of Alzheimer's Disease via the Modulation of γ-Secretase Activity. J. Alzheimers Dis. JAD. 2014 doi:10.3233/JAD-141356.
39. Robertson AL, et al. Small heat-shock proteins interact with a flanking domain to suppress polyglutamine aggregation. Proc. Natl. Acad. Sci. U. S. A. 2010; 107:10424–10429. [PubMed: 20484674]

40. Bilen J, Bonini NM. Drosophila as a model for human neurodegenerative disease. Annu. Rev. Genet. 2005; 39:153–171. [PubMed: 16285856]
41. Tue NT, Shimaji K, Tanaka N, Yamaguchi M. Effect of αB-crystallin on protein aggregation in Drosophila. J. Biomed. Biotechnol. 2012; 2012:252049. [PubMed: 22505806]
42. Williams A, et al. Novel targets for Huntington's disease in an mTOR-independent autophagy pathway. Nat. Chem. Biol. 2008; 4:295–305. [PubMed: 18391949]
44. Lejeune F-X, et al. Large-scale functional RNAi screen in C. elegans identifies genes that regulate the dysfunction of mutant polyglutamine neurons. BMC Genomics. 2012; 13:91. [PubMed: 22413862]
45. Miller JP, et al. Matrix metalloproteinases are modifiers of huntingtin proteolysis and toxicity in Huntington's disease. Neuron. 2010; 67:199–212. [PubMed: 20670829]
46. Miller JP, et al. A genome-scale RNA-interference screen identifies RRAS signaling as a pathologic feature of Huntington's disease. PLoS Genet. 2012; 8:e1003042. [PubMed: 23209424]
47. Yamanaka T, et al. Large-scale RNA interference screening in mammalian cells identifies novel regulators of mutant huntingtin aggregation. PloS One. 2014; 9:e93891. [PubMed: 24705917]
48. Waudby CA, et al. The interaction of alphaB-crystallin with mature alpha-synuclein amyloid fibrils inhibits their elongation. Biophys. J. 2010; 98:843–851. [PubMed: 20197038]
49. Raman B, et al. AlphaB-crystallin, a small heat-shock protein, prevents the amyloid fibril growth of an amyloid beta-peptide and beta2-microglobulin. Biochem. J. 2005; 392:573–581. [PubMed: 16053447]
50. Hochberg GKA, et al. The structured core domain of αB-crystallin can prevent amyloid fibrillation and associated toxicity. Proc. Natl. Acad. Sci. U. S. A. 2014; 111:E1562–1570. [PubMed: 24711386]
51. Freeman M. Reiterative use of the EGF receptor triggers differentiation of all cell types in the Drosophila eye. Cell. 1996; 87:651–660. [PubMed: 8929534]
52. Narain Y, Wyttenbach A, Rankin J, Furlong RA, Rubinsztein DC. A molecular investigation of true dominance in Huntington's disease. J. Med. Genet. 1999; 36:739–746. [PubMed: 10528852]
53. D'Agostino M, et al. The cytosolic chaperone α-crystallin B rescues folding and compartmentalization of misfolded multispan transmembrane proteins. J. Cell Sci. 2013; 126:4160–4172. [PubMed: 23843626]
54. Renna M, Caporaso MG, Bonatti S, Kaufman RJ, Remondelli P. Regulation of ERGIC-53 gene transcription in response to endoplasmic reticulum stress. J. Biol. Chem. 2007; 282:22499–22512. [PubMed: 17535801]
55. Howarth JL, et al. Hsp40 molecules that target to the ubiquitin-proteasome system decrease inclusion formation in models of polyglutamine disease. Mol. Ther. J. Am. Soc. Gene Ther. 2007; 15:1100–1105.
56. Kimmel CB, Ballard WW, Kimmel SR, Ullmann B, Schilling TF. Stages of embryonic development of the zebrafish. Dev. Dyn. Off. Publ. Am. Assoc. Anat. 1995; 203:253–310.
57. Hyatt GA, Schmitt EA, Fadool JM, Dowling JE. Retinoic acid alters photoreceptor development in vivo. Proc. Natl. Acad. Sci. U. S. A. 1996; 93:13298–13303. [PubMed: 8917585]

Europe PMC Funders Author Manuscripts

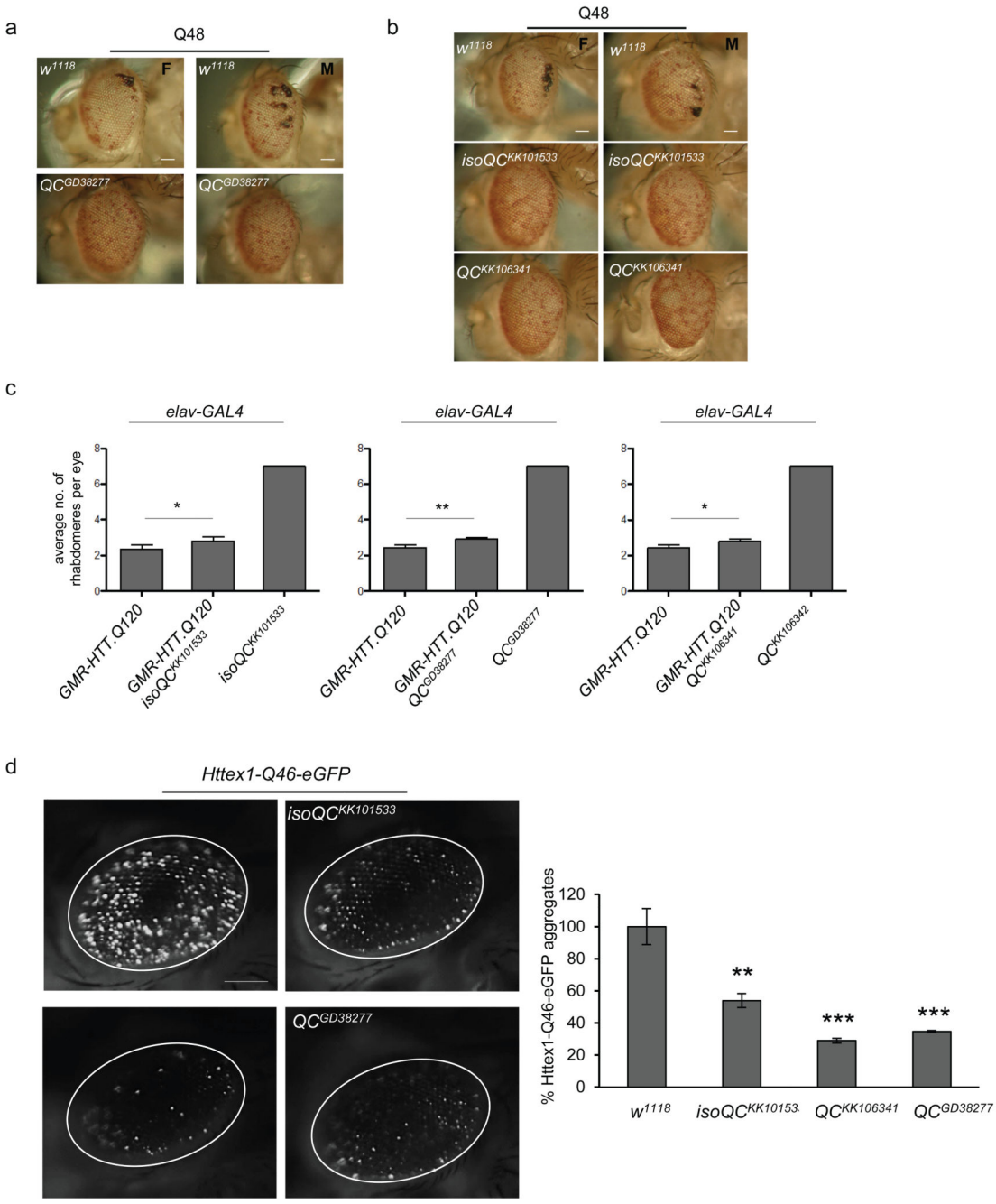

Figure 1. Downregulation of QPCT in flies rescues HD toxicity

a. The eye phenotype of flies that express Q48 crossed to w^{1118} (VDRC stock number 60000) is rescued upon downregulation of *Drosophila Glutaminyl cyclase* ($QC^{GD38277}$, VDRC GD-RNAi line 38277). Representative images of eye pigmentation rescue are shown. F=female; M=male.

b. Downregulation of QPCT fly orthologs *QC* and *isoQC* using KK-RNAi lines (lines $QC^{KK106341}$ and $isoQC^{KK101533}$) reduced the number of black necrotic-like spots on Q48 flies (see Supplementary Fig.5a for quantification). Fisher's exact test was applied for

statistical comparison between control and test genotypes. Females: $isoQC^{KK101533}$ p=2.42 E-14; $QC^{KK106341}$ p= 3.05 E-12; males: $isoQC^{KK101533}$ p=3.53 E-0.8; $QC^{KK106341}$ p= 1.72 E-0.9

c. Loss of rhabdomeres due to expression of expanded huntingtin exon1 (*elav-Gal4; GMRHTT.Q120*) in the eye was significantly rescued upon downregulation of QPCT fly orthologues *QC* or *isoQC* (GD- or KK-RNAi lines as indicated). Graph shows the mean ± SEM of the average number of rhabdomeres per eye from 4 independent experiments; one-tailed paired t-test was used to test significance.

d. The number of aggregates in the eyes of flies expressing expanded huntingtin HTTex1-Q46-eGFP using GMR-GAL4 was reduced by downregulating QPCT fly orthologs *QC* and *isoQC (*RNAi lines $isoQC^{KK101533}$, $QC^{KK10634}$, $QC^{GD38277}$). Graph shows mean ± SEM of the number of aggregates from 4 independent crosses for each genotype with control levels set at 100%. One-tailed paired t-test was used for comparison between control and test genotypes (n = 4).

In all panels, * p<0.05, ** p<0.01 and *** p<0.001. Scale bars represent 200 μm.

Europe PMC Funders Author Manuscripts

Europe PMC Funders Author Manuscripts

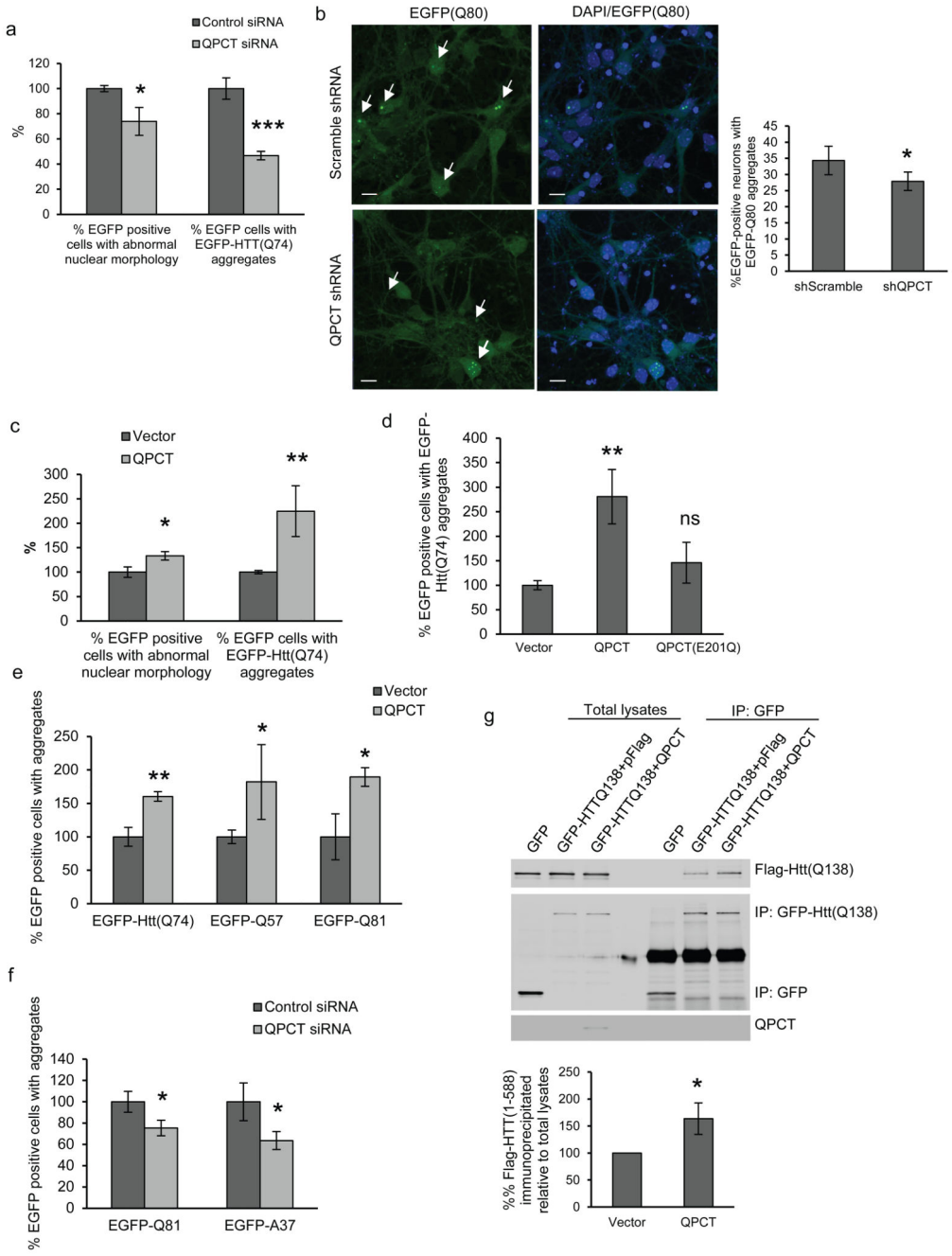

Figure 2. QPCT modulates HTT toxicity and aggregation in mammalian cell lines and primary neurons

a. The percentage of cells with apoptotic nuclei or HTT(Q74) aggregates is reduced in HEK293 cells transiently expressing EGFP-HTT(Q74) and treated with QPCT siRNA. Representative images are shown in supplementary figure 6a.

b. QPCT shRNA significantly reduced the number of aggregates in mouse primary cortical neurons expressing Q80-EGFP. Scale bar represents 10 μm. The mean of 3 independent experiments in triplicate is represented in the graph. Significance was analysed by two-tailed paired Student's t-test.

Europe PMC Funders Author Manuscripts

c,d. Overexpression of QPCT (*pCMV6-QPCT*) together with EGFP-HTT(Q74) in HeLa cells for 48h increased the percentage of cells with apoptotic nuclear morphology and aggregates (**c**), this effect is not observed with a catalytically inactive QPCT (QPCT(E201Q)-Flag) (**d**).

e. The percentage of HeLa cells expressing EGFP-HTT(Q74), EGFP-Q57 or EGFP-Q81 with aggregates is enhanced upon QPCT-Flag overexpression for 48 h.

f. QPCT siRNA reduces the percentage EGFP-Q81 or EGFP-A37 with aggregates in HEK293.

g. Overexpression of QPCT enhanced the amount of mutant HTT(1-548)-Flag co-immunoprecipitating with HTT(1-588)-GFP. Levels of Flag-HTT(1-588) co-immunoprecipitated relative to total lysates from 5 independent experiments are represented in the graph. Data were analyzed by two-tailed paired Student's t-test (n= 5 experiments). Full blot images are shown in Supplementary Fig. 17a.

In all panels, unless indicated, graphs show mean values with control conditions set to 100 and error bars represent standard deviation from a triplicate experiment representative of at least three independent experiments. Statistical analyses were performed by two-tailed unpaired Student's t-test: ***p<0.001, **p<0.01; *p<0.05; NS, not significant

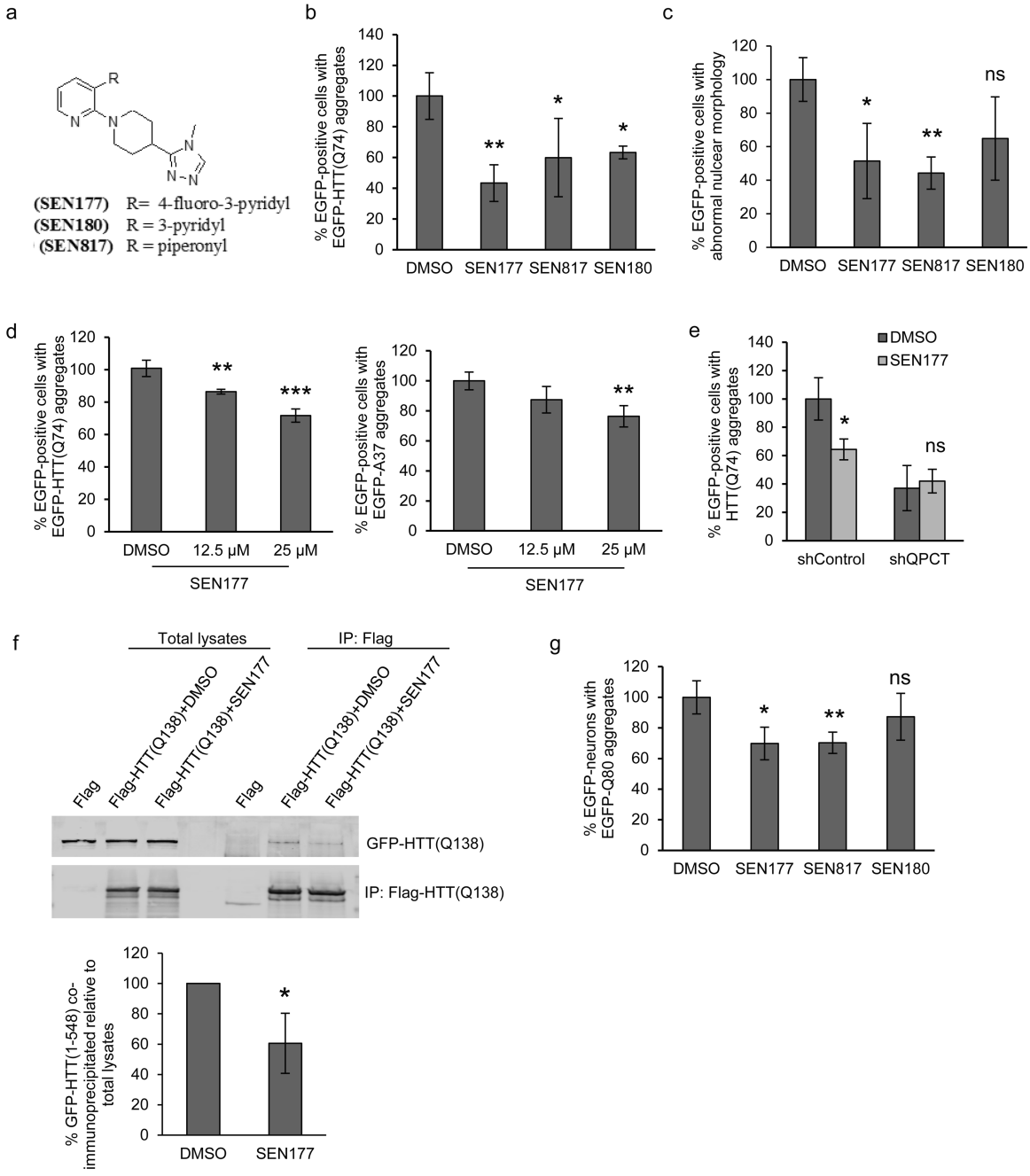

Figure 3. Design of QPCT inhibitors that reduce mutant HTT aggregation

a. Chemical structure of compounds designed to inhibit QPCT activity. Table indicating the activity and in vitro ADME properties of the compounds is shown in supplementary fig. 11a.

b,c. Treatment of HeLa cells expressing EGFP-HTT(Q74) with SEN177, 817 and 180 (50 μM) for 24h reduced the percentage of cells with aggregates (**b**) and apoptotic nuclei (**c**).

d. SEN177 reduces the percentage of HEK293 cells with EGFP-HTT(Q74) or EGFP-A37 aggregates in a concentration-dependent manner.

Europe PMC Funders Author Manuscripts

e. SEN177 does not further reduce the percentage of EGFP-HTT(Q74) aggregates in QPCT shRNA transfected cells.

f. SEN177 reduces the amount of HTT(1-588)-GFP co-immunoprecipitating with HTT(1-548)-Flag in HeLa cells (25 μM SEN177). The amount of GFP-HTT(1-548) immunoprecipitated relative to total lysates was quantifiedand the average of 5 independent experiments is shown in the graph. Data were analyzed by two-tailed paired Student's t-test (n= 5 experiments). Full blot images are shown in Supplementary information 17b.

g. Primary neurons expressing EGFP-Q80 for 3 days were treated with 50 μM of indicated compounds for further 24h.

In all panels, unless indicated, graphs show mean values with control conditions set to 100 and error bars represent standard deviation from a triplicate experiment representative of at least three independent experiments. Statistical analyses were performed by two-tailed unpaired Student's t-test: ***$p<0.001$, **$p<0.01$; *$p<0.05$; NS, not significant.

Europe PMC Funders Author Manuscripts

Europe PMC Funders Author Manuscripts

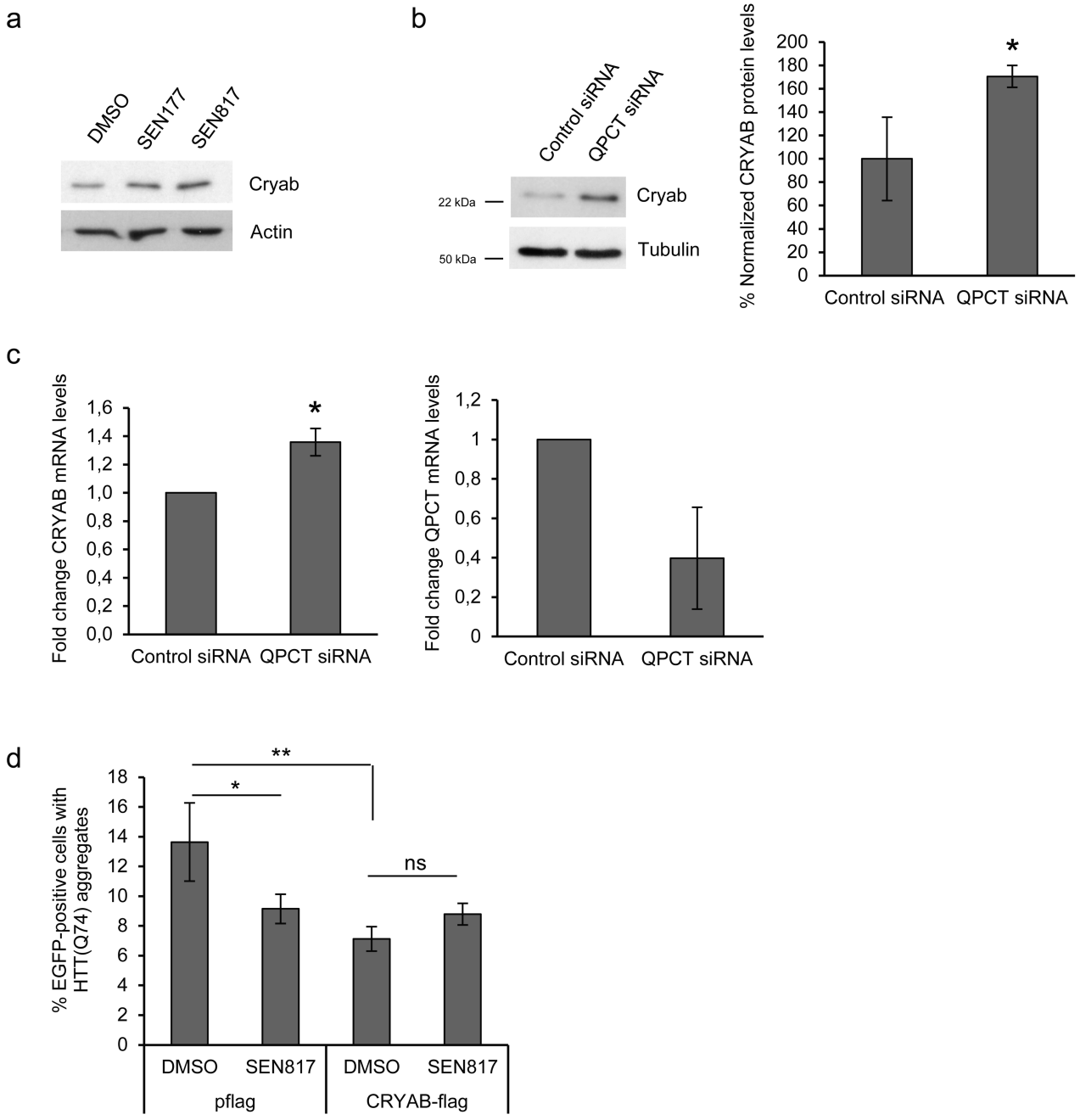

Figure 4. QPCT inhibition induces alpha B-crystallin levels

a. Alpha B-crystallin (Cryab) protein levels were increased in cells transfected with HTT(Q74)GFP and treated with the indicated compounds at 25 μM for 24 h. Full blot images are shown in Supplementary information 17c.

b,**c**. Knockdown of QPCT for 24 h followed by transfection with HTT(Q74)GFP for another 24h increased protein (**b**) and mRNA (**c**) levels of alpha B-crystallin. Fold change in mRNA of QPCT or alpha B-crystallin is represented in the graph with error bars representing standard deviation. The mean of three independent experiments in triplicate was normalized

to 1 and significance was calculated by one sample t-test. Full blot images are shown in Supplementary information 17d.

d. Overexpression of alpha B-crystallin (CRYAB-Flag) reduced the percentage of cells with HTT(Q74)GFP aggregates. SEN817 decreased aggregation when added at 25 μM for 24h in control but not CRYAB-expressing cells. In all panels, unless indicated, graphs show mean values with control conditions set to 100 or 1, and error bars represent standard deviation from a triplicate experiment representative of at least three independent experiments. Statistical analyses were performed by two-tailed unpaired Student's t-test: $^{**}p<0.01$; $^{*}p<0.05$; NS, not significant.

Europe PMC Funders Author Manuscripts

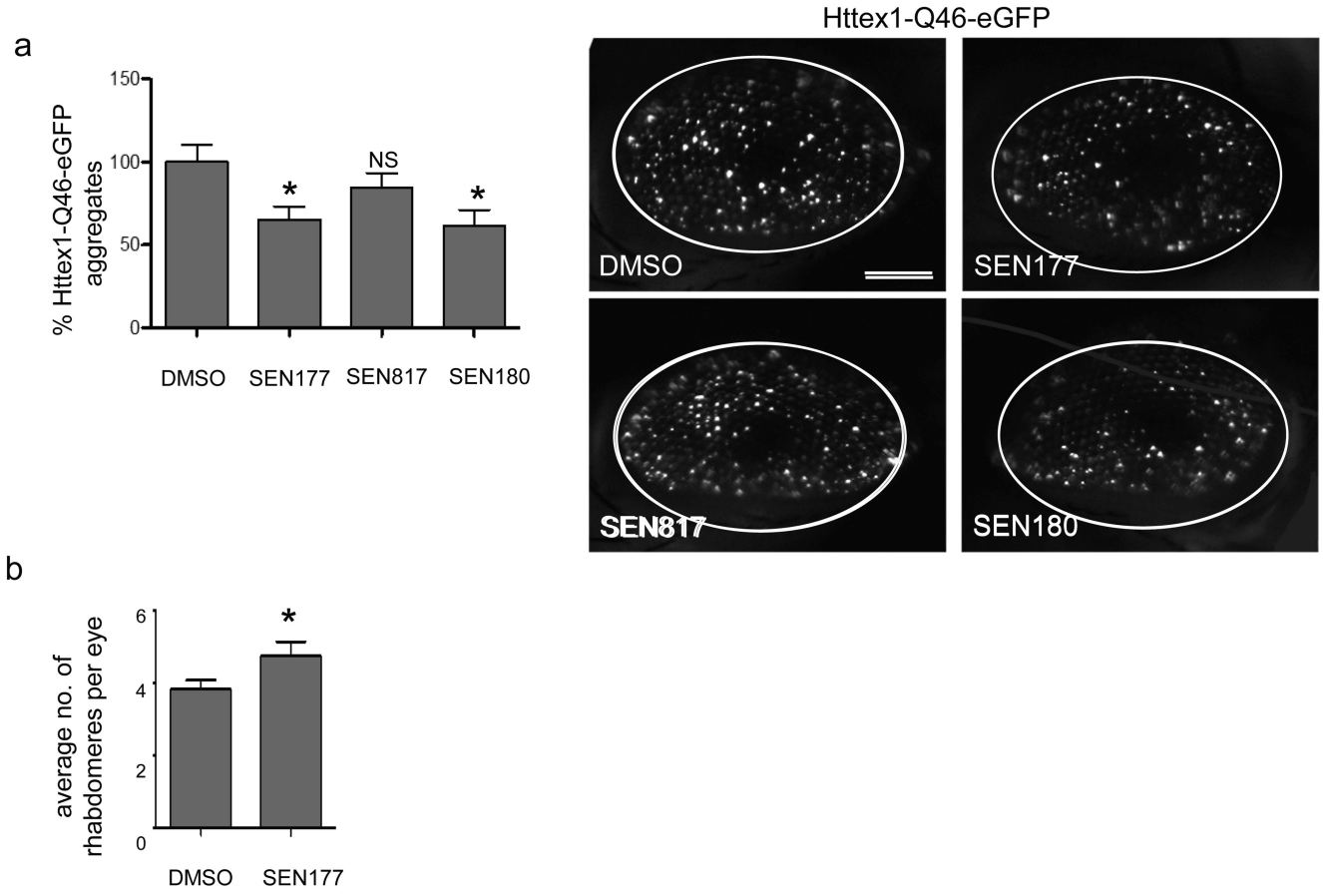

Figure 5. Pharmacologic inhibition of QPCT in fly

a. Flies that expressed HTTex1-Q46-eGFP in the eye have fewer aggregates after treatment with 50 μM of indicated compounds . Graph represents mean ± SEM from 4 independent crosses for each compound. Statistical analyses were performed by one-tailed unpaired Student's t-test. Scale bars represent 200 μm.

b. Flies expressing HTTEx1-Q120 (*GMR-HTT.Q120*) show more rhabdomeres after treatment with SEN177 (50 μM). Graph represents the average number of rhabdomeres per eye ±SEM from 3 independent experiments with females and males counted separately, each based on approximately 10 individuals per datapoint, scoring 15 ommatidia from each individual. Statistical analysis was performed using one-tailed paired Student's t-test.

Europe PMC Funders Author Manuscripts

Europe PMC Funders Author Manuscripts

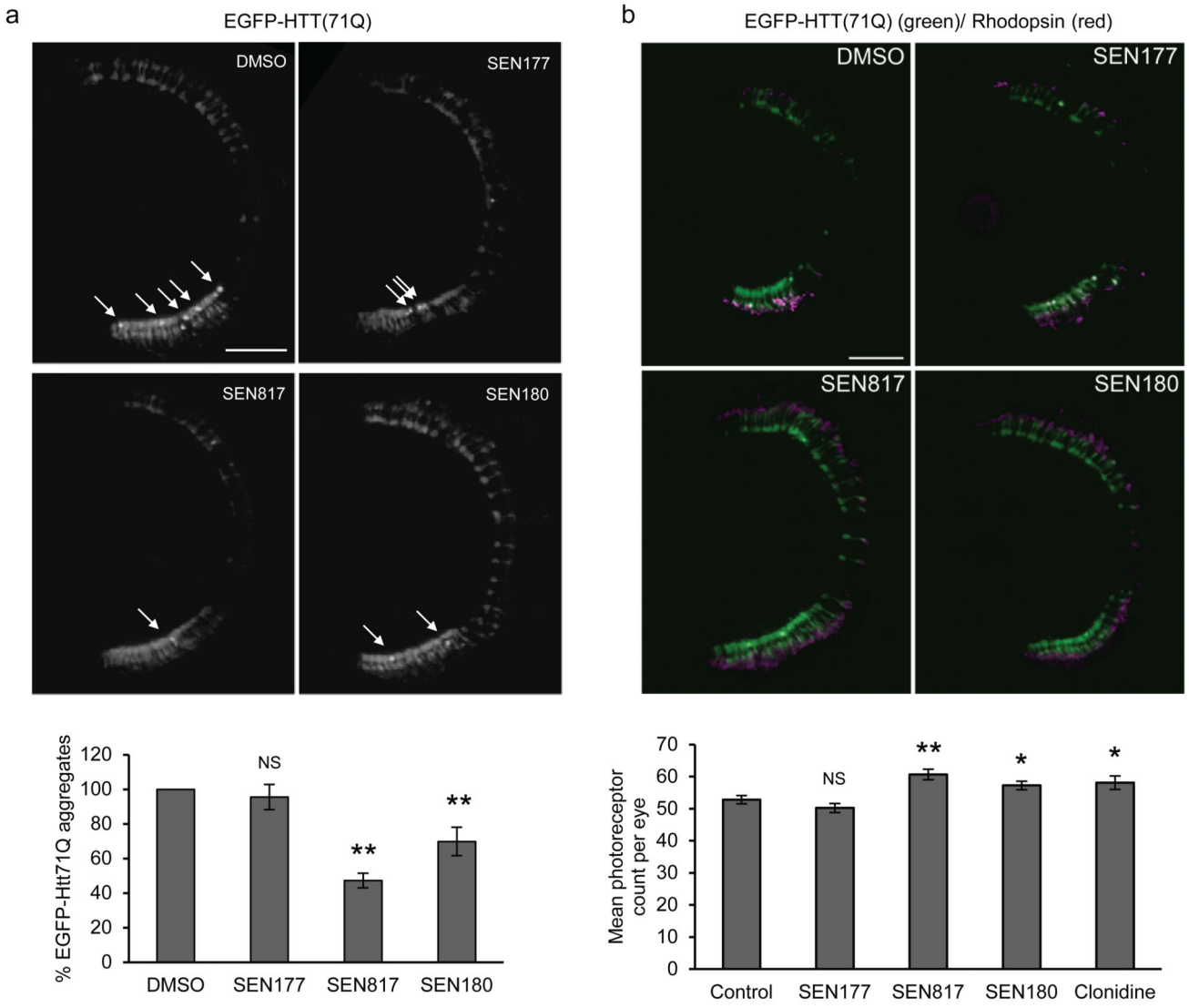

Figure 6. Pharmacologic inhibition of QPCT in zebrafish

a. Representative sections through the central retina of transgenic HD zebrafish at 7 d.p.f. treated with DMSO, SEN177 (1 mM), SEN817 (100 μM) or SEN180 (100 μM) showing aggregates (arrow) within the rod photoreceptors. Scale bar represents 10 μm. Treatment with QPCT inhibitors resulted in reduction in aggregates (Student's t-test) for SEN187 and SEN810.

b. Representative sections through the central retina of transgenic HD zebrafish at 9 d.p.f. treated with DMSO, SEN177 (1 mM), SEN817 (100 μM) or SEN180 (100 μM). To demonstrate that loss of GFP corresponds to loss of photoreceptors, sections were stained with anti-rhodopsin (1D1) antibody (red). GFP labels the whole rod photoreceptor, whereas rhodopsin is present in the rod outer segment. Merged images show co-localisation of GFP the rhodopsin (red). Photoreceptor degeneration is ameliorated by SEN817 and SEN180. Scale bars, 10 μm.

In all panels, **$p<0.01$; *$p<0.05$; NS, not significant.

Europe PMC Funders Author Manuscripts